Scaling Function, Spectral Function and Nucleon Momentum Distribution in Nuclei

A.N. Antonov[1], **M.V. Ivanov**[1,2], **J.A. Caballero**[3], **M.B. Barbaro**[4], **J.M. Udias**[2], **E. Moya de Guerra**[2], **T.W. Donnelly**[5]

[1] Institute for Nuclear Research and Nuclear Energy, Bulgarian Academy
of Sciences, Sofia 1784, Bulgaria
[2] Departamento de Fisica Atomica, Molecular y Nuclear, Facultad de Ciencias
Fisicas, Universidad Complutense de Madrid (UCM), Madrid E-28040, Spain
[3] Departamento de Física Atómica, Molecular y Nuclear, Universidad de Sevilla,
41080 Sevilla, SPAIN
[4] Dipartimento di Fisica Teorica, Università di Torino and INFN,
Sezione di Torino, Via P. Giuria 1, 10125 Torino, Italy
[5] Center for Theoretical Physics, Laboratory for Nuclear Science and
Department of Physics, Massachusetts Institute of Technology,
Cambridge, MA 02139, USA

Abstract. The aim of the study is to find a good simultaneous description of the spectral function and the momentum distribution in relation to the realistic scaling function obtained from inclusive electron-nuclei scattering experiments. We start with a modified Hartree-Fock spectral function in which the energy-dependent part (δ-function) is replaced by the Gaussian distributions with hole-state widths as free parameters. We calculate the scaling function and the nucleon momentum distribution on the basis of the spectral function constructed in this way, trying to find a good description of the experimental data. The obtained scaling function has a weak asymmetry and the momentum distribution has not got a high-momentum tail in the case when harmonic-oscillator single-particle wave functions are used. So, to improve the behavior of the momentum distribution we used the basis of natural orbitals (NO) in which short-range correlations are partly incorporated. The results for the scaling function show again a weak asymmetry, but in this case the momentum distribution has a high-momentum tail. As a next step we include final-state interactions (FSI) in the calculations to reproduce the experimentally observed asymmetry of the scaling function.

1 Introduction

Inclusive scattering of high energy electrons off nuclear targets has long been recognized as a powerful tool to measure the nucleon momentum $n(k)$ and removal energy distribution [1–3]. The underlying picture is that at large momentum transfer electron-nucleus scattering reduces to the incoherent sum of elementary scattering processes involving individual nucleons, distributed in momentum and removal energy according to the spectral function $S(p, \mathcal{E})$. Thus,

the data of inclusive quasielastic (QE) electron-nucleus scattering provide tests for the nuclear many-body theory. This concerns mainly the possibility to establish the validity of the mean-field approximation (MFA) and the role of the nucleon-nucleon correlations on the characteristics of the nuclear structure and reactions, as well as the effects of the Final State Interactions (FSI) on the nuclear processes. As known, using the shell model, it is possible in principle to obtain the contributions of different shells to $S(p, \mathcal{E})$ and the momentum distribution for each single-particle state. However, due to the residual interactions, the hole states are not eigenstates of the residual nucleus but are mixtures of several single-particle states. This leads to the spreading of the shell structure and only a careful study of the momentum dependence of $S(p, \mathcal{E})$ can separate the contributions from different shells (see, *e.g.* [4]). Such analyses have been carried out for few-body systems, complex nuclei and nuclear matter and they have been concentrated mainly on the existence of high-momentum components of the nucleon momentum distribution due to nucleon-nucleon (NN) correlation effects [2–7]. This problem is of particular importance because, as is known ([4, 7–11]) it is impossible within the MFA to describe simultaneously the density and momentum distributions in nuclei, so consistent analysis of the role of the NN correlations is required using theoretical methods beyond the MFA in the description of the results of relevant experiments.

In the early seventies, West first pointed out [12] that, if the electron-nucleon processes are elastic and the final state state interactions between the struck particle and the spectator system can be neglected, the nuclear response $R(\mathbf{q}, \omega)$, which generally depends upon both momentum ($\mathbf{q}$) and energy (ω) transfer, exhibits scaling, *i.e.* it can be simply related to a function of only one kinematical variable, denoted y. Within the simplest nonrelativistic approximation, y can be identified with the minimum projection of the nucleon momentum along the direction of the momentum transfer, while the scaling function $F(y) = (q/m)R(\mathbf{q}, \omega)$, where m denotes the nucleon mass, can be directly written in terms of the nucleon momentum distribution. Our study uses the results concerning the y-scaling ([1–3, 12–14]) and superscaling (based on ψ'-scaling variable (*e.g.* [14–22]) obtained from the analyses of the vast amount of inclusive electron scattering world data. Scaling of the first kind of the introduced scaling function $f(\psi')$ (*i.e.* no dependence of ψ' and $f(\psi')$ on the momentum transfer q) is observed at excitation energies below the QE peak. Scaling of second kind (*i.e.* no dependence on the mass number) turns out to be excellent in the same region. When scaling of both first and second types occur, one says that superscaling takes place. It was pointed out (ses, *e.g.* [17, 19–22]) that the physical reason of the superscaling is the specific high-momentum tail of $n(p)$ which arises due to NN correlations and is similar for all nuclei. As was pointed out in [23], however, the connection between the scaling function extracted from the analysis of the cross-section data, and the spectral function only exists assuming very restricted approximations. Along this line, caution should be kept in mind for the conclusions reached about the momentum distribution, because a

close relationship between the latter and the scaling function only emerges after some approximations are made. These are linked particularly to the integration limits involved and the behavior of the spectral function [1]. In [23] the analysis applied in the past to the scaling region (that is, negative values of the scaling variable y) was extended to positive y and it led to results that differ from those solely on the y-scaling region and provide a new insight on the problem how the energy and momentum are distributed in the spectral function.

As is known (*e.g.* [23] and references therein) in the Plane Wave Impulse Approximation (PWIA) the $(e, e'N)$ differential cross section factorizes in the form:

$$\left[\frac{d\sigma}{d\epsilon' d\Omega' dp_N d\Omega_N} \right]^{PWIA}_{(e,e'N)} = K\sigma^{eN}(q, \omega; p, \mathcal{E}, \phi_N) S(p, \mathcal{E}) , \tag{1}$$

where σ^{eN} is the electron-nucleon cross section for a moving off-shell nucleon, $S(p, \mathcal{E})$ is the spectral function that gives the probability to find a nucleon of certain momentum and energy in the nucleus (see *e.g.* [24–26]) and K is a kinematical factor [27]. In Eq. (1) p is the missing momentum and $\mathcal{E}$ is the excitation energy that is essentially the missing energy minus the separation energy. Further assumptions are necessary [23] to show how the scaling function $F(q, \omega)$ emerges from the PWIA, namely, the spectral function is assumed to be isospin independent and σ^{eN} is assumed to have a very mild dependence on p and $\mathcal{E}$. The scaling function can be expressed by the differential cross section of inclusive QE (e, e') processes:

$$F(q, \omega) \cong \frac{[d\sigma/d\epsilon' d\Omega']_{(e,e')}}{\overline{\sigma}^e(q, \omega; p = |y|, \mathcal{E} = 0)} . \tag{2}$$

In Eq. (2) $\overline{\sigma}^e$ is taken at $p = |y|$, where the scaling variable y is the smallest value of the missing momentum p that can occur in the processes of electron-nuclei scattering for the smallest possible value of the missing energy ($\mathcal{E} = 0$). It is azimuthal angle-averaged single-nucleon cross section that also incorporates the kinematical factor K:

$$\overline{\sigma}^e \equiv K \sum_{i=1}^{A} \int d\phi_{N_i} \frac{\sigma^{eN_i}}{2\pi} . \tag{3}$$

So, in the PWIA the scaling function $F(q, \omega)$ from Eq. (2) is expressed in terms of the spectral function:

$$F(q, \omega) = 2\pi \iint_{\Sigma(q,\omega)} p \, dp \, d\mathcal{E} \, S(p, \mathcal{E}) , \tag{4}$$

where $\Sigma(q, \omega)$ presents the kinematically allowed region (for details, see *e.g.* [23]). As known, only in the case when it is possible to extend the region $\Sigma(q, \omega)$ to

infinity in the excitation energy plane (*i.e.* at $\mathcal{E}_{\max} \to \infty$), the scaling function would be directly linked to the momentum distribution of the A-nuclear system:

$$n(p) = \int_0^\infty d\mathcal{E} S(p, \mathcal{E}). \tag{5}$$

It was shown from the analyses of the inclusive electron-nucleus scattering that at high values of the momentum transfer ($q > 500$ MeV/c) the extracted scaling function $F_{\exp}(q, \omega)$ becomes only a function of the scaling variable y [$F_{\exp}(q, y)$] [1, 16–18]. It was emphasized in [23] that Eq. (4) does not apply to $F_{\exp}(q, \omega)$ if it has ingredients not included in the PWIA, such as final-state interactions, meson exchange currents, rescattering processes *etc.*

Introducing the separate longitudinal (L) and transverse (T) (e, e') data made it possible to introduce a "universal" experimental dimensionless superscaling function (using the Relativistic Fermi gas (RFG) model):

$$f_{\exp}(q, \omega) \equiv k_F F_{\exp}(q, \omega); \; f_{\exp}^{L(T)}(q, \omega) \equiv k_F F_{\exp}^{L(T)}(q, \omega), \tag{6}$$

k_F being the Fermi momentum. We note, however, that the effects of FSI and relativity on this function are important and, as emphasized in [23], any conclusion about the momentum distribution based on Eq. (4) should be made with caution.

In the present work we study in more details the relationship between the spectral function $S(p, \mathcal{E})$ and the scaling function $F(q, y)$ and try to extract information about the spectral function from the experimentally known scaling function keeping in mind the restrictions of the PWIA. We take into account the effects of FSI and some other peculiarities of the electron-nuclei scattering mechanism. We make an attempt to construct the spectral function that corresponds to the experimentally established scaling function following subsequent steps. Firstly, we consider $S(p, \mathcal{E})$ within and beyond the MFA (Hartree-Fock method and beyond it) within the PWIA. Secondly, we take into account the FSI calculating the inclusive electron-nucleus cross section using the Dirac optical potential and determine the spectral function in this case as well. In all steps we relate the obtained results for the scaling function to the empirically obtained one. We establish a relationship of the obtained single-particle widths in the approach to the experimental ones.

The theoretical scheme, the numerically obtained results and the discussion are given in Section 2. The conclusions are presented in Section 3.

2 Scaling Function in Relation to Spectral Function and Momentum Distributions

In this Section we give the main relationships used in our approach to find a good simultaneous description of the spectral function, the momentum distribution and the scaling function. As mentioned in the Introduction, the scaling function

is given in the PWIA by Eq. (2) as a ratio between the inclusive electron cross section and the electron-nucleon cross section at $p = |y|$ and $\mathcal{E} = 0$. Also in the PWIA the scaling function is expressed in terms of the spectral function by Eq. (4). It was shown in [23] that in this scheme the equations that relate the scaling function $F(q, y)$ with the spectral function in PWIA in the regions of negative and positive values of the scaling variable y have the form:

$$\frac{1}{2\pi} F(q, y) = \int_{-y}^{Y(q,y)} p\, dp \int_{0}^{\mathcal{E}^-(p;q,y)} d\mathcal{E}\, S(p, \mathcal{E}) \qquad \text{if } y < 0 \quad (7)$$

$$\frac{1}{2\pi} F(q, y) = \int_{0}^{y} p\, dp \int_{\mathcal{E}^+(p;q,y)}^{\mathcal{E}^-(p;q,y)} d\mathcal{E}\, S(p, \mathcal{E})$$

$$+ \int_{y}^{Y(q,y)} p\, dp \int_{0}^{\mathcal{E}^-(p;q,y)} d\mathcal{E}\, S(p, \mathcal{E}) \qquad \text{if } y > 0 \quad (8)$$

In Eqs. (7) and (8):

$$y(q, \omega) = \left\{ (M_A^0 + \omega)\sqrt{\Lambda^2 - M_B^{0^2} W^2} - q\Lambda \right\} / W^2, \qquad (9)$$

$$Y(q, \omega) = \left\{ (M_A^0 + \omega)\sqrt{\Lambda^2 - M_B^{0^2} W^2} + q\Lambda \right\} / W^2, \qquad (10)$$

$$\mathcal{E}^{\pm}(p; q, \omega) = (M_A^0 + \omega) - \left[\sqrt{(q \pm p)^2 + m_N^2} + \sqrt{M_B^{0^2} + p^2} \right], \quad (11)$$

where ω is the energy transfer, M_A^0 is the target nuclear mass, m_N is the nucleon mass, M_B^0 is the ground-state mass of the residual nucleus, $\Lambda \equiv (M_B^{0^2} - m_N^2 + W^2)/2$ with $W \equiv \sqrt{(M_A^0 + \omega)^2 - q^2}$ being the center-of-mass energy.

In the Relativistic Fermi Gas model the dimensionless scaling variable ψ is introduced [14–17] in the form:

$$\psi = \frac{1}{\sqrt{\xi_F}} \frac{\lambda - \tau}{\sqrt{(1 + \lambda)\tau + \kappa\sqrt{\tau(1 + \tau)}}}, \qquad (12)$$

where $\eta_F = k_F/m_N$, k_F is the Fermi momentum, $\xi_F = \sqrt{1 + \eta_F^2} - 1$ is the dimensionless Fermi kinetic energy, $\kappa = q/(2m_N)$, $\lambda = \omega/(2m_N)$, and $\tau = |Q^2|/(4m_N^2) = \kappa^2 - \lambda^2$ is the dimensionless absolute value of the squared 4-transferred momentum. The physical meaning of ψ^2 (in units of the Fermi energy) is the smallest kinetic energy that one of the nucleons responding to an external probe can have. In studies of electron scattering scaling one usually includes a small energy shift by replacing ω by $\omega - E_{\text{shift}}$ in order to force the maximum of the QE response to occur for $\psi' = 0$ (see, for example, [16–18]). This is equivalent to taking $\lambda \to \lambda' = \lambda - \lambda_{\text{shift}}$ with $\lambda_{\text{shift}} = E_{\text{shift}}/2m_N$ and correspondingly $\tau \to \tau' = \kappa^2 - \lambda'^2$ in Eq. (12).

The scaling variables y and ψ are closely related [16, 17]:

$$\psi = \left(\frac{y}{k_F}\right)\left[1 + \sqrt{1 + \frac{m_N^2}{q^2}\frac{1}{2}\eta_F\left(\frac{y}{k_F}\right)} + \mathcal{O}[\eta_F^2]\right] \simeq \frac{y}{k_F}. \qquad (13)$$

The dimensionless scaling function $f(\psi)$ is introduced (*e.g.* [17]) in the RFG model:

$$f_{\text{RFG}}(\psi) = k_F F_{\text{RFG}}(\psi) \simeq \frac{3}{4}\left(1 - \psi^2\right)\Theta\left(1 - \psi^2\right). \qquad (14)$$

As shown in the RFG model, at sufficiently high momentum q (> 500 MeV/c) $f(\psi)$ depends only on ψ and not on the transfer momentum q (thus showing scaling of the first kind) as well as $f(\psi)$ and ψ are independent of the mass number A for a wide range of nuclei from ^{4}He to ^{197}Au (showing scaling of the second kind), so the scaling function $f_{\text{RFG}}(\psi)$ exhibits superscaling. As mentioned in the Introduction, in the case in which it is possible to extend the kinematically allowed region $\Sigma(q, \omega)$ to infinity in the excitation energy plane, that is $\mathcal{E}_{\text{max}} \to \infty$, the scaling function can be linked directly to the true momentum distribution of the A-nuclear system (see Eq. (5)).

2.1 Spectral Function in the Hartree-Fock Method and Beyond It

As noted in the Introduction the aim of the present work is to construct realistic spectral function that leads to a good agreement with the scaling function obtained from the inclusive electron-nuclei scattering data. We start with a given form of the spectral function, *e.g.* that in the Hartree-Fock method:

$$S_{HF}(p, \mathcal{E}) = \sum_i 4(2l_i + 1)n_i(p)\delta(\mathcal{E} - \mathcal{E}_i), \qquad (15)$$

where $n_i(p)$ is the momentum distribution of the shell-model single-particle state i and $\mathcal{E}_i$ is the single-particle energy. As a next step we construct a more complicated spectral function in which the energy-dependent part in Eq. (15) (the δ-function) is replaced by the Gaussian distribution $G_{\sigma_i}(\mathcal{E} - \mathcal{E}_i)$:

$$S(p, \mathcal{E}) = \sum_i 4(2l_i + 1)n_i(p)G_{\sigma_i}(\mathcal{E} - \mathcal{E}_i), \qquad (16)$$

where

$$G_{\sigma_i}(\mathcal{E} - \mathcal{E}_i) = \frac{1}{\sigma_i\sqrt{\pi}}e^{-\frac{(\mathcal{E} - \mathcal{E}_i)^2}{\sigma_i^2}} \qquad (17)$$

and σ_i is a parameter for a given single-particle state i that is related to the width of the hole state i. For the ^{16}O nucleus we consider two parameters σ_{1s} and σ_{1p} that are related to the widths of the $1s$ and $1p$ hole states, respectively. In the calculations we are looking for a best fit of these parameters that gives a good description of the experimental data for the scaling function $f(\psi')$, for the
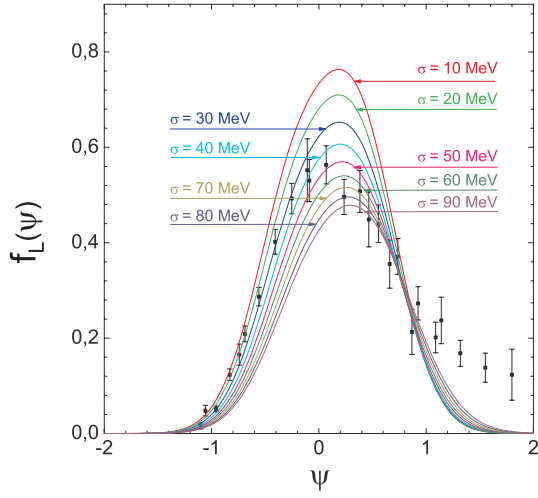
Figure 1. The results for the scaling function $f(\psi)$ (for $\sigma = 10$–90 MeV) are compared with the experimental data.

experimental values for the widths of the hole states and the high-momentum tail of the momentum distribution.

We started our calculations taking $n_i(p)$ to be the momentum distribution of the harmonic-oscillator shell-model single-particle state i. Let firstly $\sigma_{1s} = \sigma_{1p} = \sigma$ and let σ varies in the region $\sigma = 10$–90 MeV. In Figure 1 are given the results for the scaling function compared with the longitudinal experimental data.

Our next step was to calculate the scaling function $f(\psi')$ at fixed values of σ_{1s} and varying $\sigma_{1p} = 10$–90 MeV. The results are given in Figure 2 for $\sigma_{1s} = 10$ and 90 MeV and σ_{1p} varying between 10 and 90 MeV.
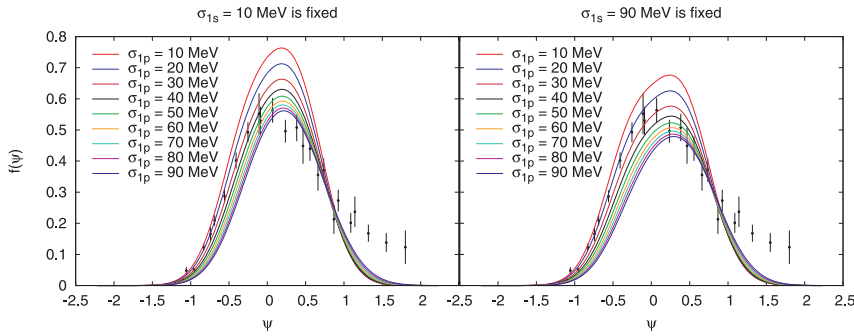
Figure 2. The results for the scaling function $f(\psi)$ (for $\sigma_{1s} = 10$ and 90 MeV and σ_{1p} varying between 10 and 90 MeV) are compared with the experimental data.
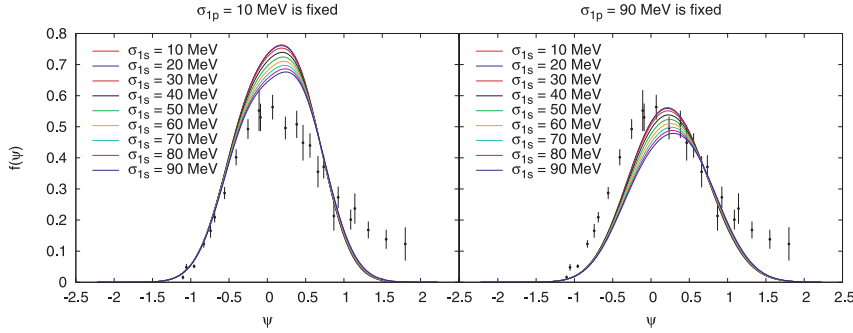
Figure 3. The results for the scaling function $f(\psi)$ (for $\sigma_{1p} = 10$ and 90 MeV and σ_{1s} varying between 10 and 90 MeV) are compared with the experimental data.

In the next Figure 3 we give the results when σ_{1p} is fixed (*e.g.* $\sigma_{1p} = 10$ and 90 MeV) while σ_{1s} is varying from 10 to 90 MeV.

One can see that at fixed values of the parameter σ_{1s} and $\sigma_{1p} = 10$–90 MeV the main changes of the scaling function are observed in the form and the maximum value. Unlike, in the case of fixed values of σ_{1p} and $\sigma_{1s} = 10$–90 MeV, the main changes of the scaling function are visible in the maximum, but not in the form.

The momentum distribution calculated by Eq. (5) is the HF momentum distribution, so in this first attempt (using HO single-particle wave functions) it is impossible the momentum distribution to have a high-momentum tail. In this aspect, our next step is to use natural orbitals (NO's) for the single-particle wave functions and occupation numbers taken from a method where short-range NN correlations are accounted for. For example, we use the NO representation of the one-body density matrix (OBDM) obtained within the lowest-order approximation of the Jastrow correlation method [28].

The NO's $\phi_\alpha(r)$ are defined [29] as the complete orthonormal set of single-particle wave functions that diagonalize the OBDM:

$$\rho(\mathbf{r}, \mathbf{r}') = \sum_a N_a \varphi_a^*(\mathbf{r}) \varphi_a(\mathbf{r}'). \tag{18}$$

The eigenvalues N_α ($0 \leqq N_\alpha \leqq 1$, $\sum_\alpha N_\alpha = A$) are the natural occupation numbers.

Our calculations were continued using NO single-particle wave functions to obtain $n_i(p)$ for the expression of the spectral function given by Eq. (16). The results for the scaling function obtained using NO's and HO single-particle wave functions for various values of the parameters σ_{1s} and σ_{1p} are given in Figure 4.

In Figure 5 the resulting nucleon momentum distributions are given and compared. One can see $n(p)$ for the RFG model, also that one calculated using HO single-particle wave functions, the NO's from the Jastrow correlated approach [28], and the result obtained with the Coherent Density Fluctuation
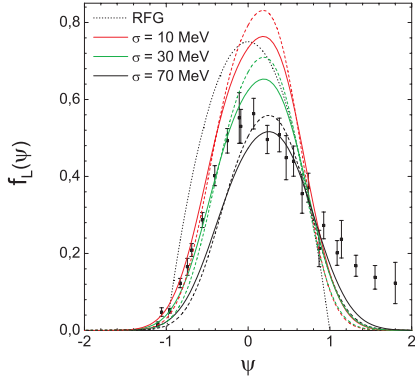
Figure 4. The results for the scaling function $f(\psi)$ obtained using NO's (dashed lines) and harmonic oscillator (HO) single-particle wave functions (solid line) for various values of the parameters $\sigma_{1s} = \sigma_{1p} = 10$ MeV (red line), 30 MeV (green line) and 70 MeV (black line).
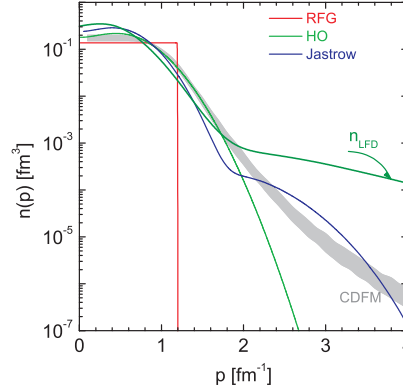
Figure 5. (Color online) The results for the momentum distribution calculated by harmonic oscillator single-particle wave functions (HO – green line); NO taken from the Jastrow model (Jastrow – blue line); Relativistic Fermi Gas (RFG – red line); CDFM results (CDFM – grey area [20, 22]); LFD results (LFD – olive line [22]).

Model (CDFM) ([4, 7, 11], see also [20, 22]). The nucleon momentum distribution n_{LFD} obtained in [22, 30] by using the Light-Front Dynamics method (LFD) [31] is given in Figure 5 as well.

2.2   Account for FSI

In this subsection we will give briefly the approach that we use in our calculations to take into account the FSI in the consideration of the spectral function, the momentum distribution and the scaling function.

As a next step we continued our study of inclusive electron-nuclei cross sections by incorporation of two types of FSI effects (following Ref. [32]): Pauli blocking and reinteraction of the struck nucleon with the spectator system described by means of the time-independent optical potential (OP):

$$U = V - \imath W \qquad (19)$$

proposed in [33]. The authors of [32] argue that the result is equivalent to making the substitution:

$$\delta(...) \to \frac{W/\pi}{W^2 + [... - V]^2} \qquad (20)$$

(see [34]) in the expression for the inclusive electron-nuclei cross section:

$$\frac{d\sigma_t}{d\omega d|\mathbf{q}|} = 2\pi\alpha^2 \frac{|\mathbf{q}|}{E_{\mathbf{k}}^2} \int dE\, d^3p\, \frac{S_t(\mathbf{p}, E)}{E_{\mathbf{p}} E_{\mathbf{p}'}} \delta(\omega + M - E - E_{\mathbf{p}'}) L_{\mu\nu}^{em} H_{em,\,t}^{\mu\nu}. \qquad (21)$$

In Eq. (21) the index t denotes the nucleon isospin, $L_{\mu\nu}^{\text{em}}$ is the leptonic tensor, $H_{\text{em},t}^{\mu\nu}$ is the hadronic tensor and $S_t(p, E)$ is the proton (neutron) spectral function.

The real and imaginary part of the OP are calculated using a Dirac OP from Ref. [35] averaging it over spatial coordinate. The potential is evaluated at root-mean-square (rms) radii from Ref. [35]. As a result the OP $U(p')$ related to the scalar (S) and vector (V) part of the potential in [35] is obtained in the form (see also [32]):

$$E_{\mathbf{p}'} + U(\mathbf{p}') = \sqrt{[M + S(T_{\mathbf{p}'}, \bar{r}_S)]^2 + \mathbf{p}'^2} + V(T_{\mathbf{p}'}, \bar{r}_V). \tag{22}$$

In Figure 6 we give the calculated real and imaginary parts of the OP $U(p')$.

Following the approach of Ref. [32] we continued our calculations of the scaling function using Eq. (2), in which the cross section in the nominator is calculated by accounting for FSI using the Dirac OP, *i.e.* exchanging the δ-function in Eq. (21) as shown in Eq. (20). The expression for $S(p, \mathcal{E})$ in Eq. (21) is taken in the form (16), where we use the momentum distributions $n_i(p)$ obtained in various cases:

i) in the RFG model,

ii) using NO's from the Jastrow correlation method.

The results in the case (i) are presented in Figure 7 for a given momentum
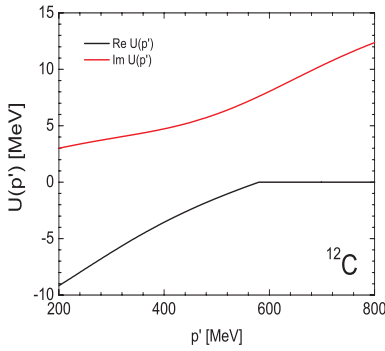
Figure 6. (Color online) The results for the real and imaginary part of the optical potential $U(p')$ for ^{12}C calculated by Eq. (22) using a Dirac OP from Ref. [35].
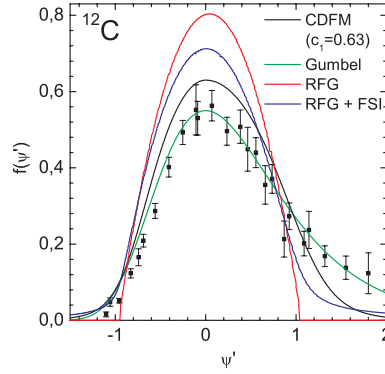
Figure 7. (Color online) The results for the scaling function $f(\psi')$ with and without accounting for the FSI in the RFG model (for a given momentum transfer $q = 1$ GeV/c and energy of the initial electron $\epsilon = 1$ GeV) are compared with the experimental data, Gumbel distribution and CDFM result using $c_1 = 0.63$ [22].

transfer $q = 1$ GeV/c and energy of the initial electron $\epsilon = 1$ GeV with and without accounting for the FSI.

The results for the scaling function $f(\psi')$ using the $S_{HF}(p, \mathcal{E})$ [Eq. (15)] with HO single-particle wave functions are presented in Figure 8 for a given momentum transfer $q = 1$ GeV/c and energy of the initial electron $\epsilon = 1$ GeV with and without accounting for the FSI. In this case we consider two different types of the time-independent optical potential for ^{16}O: obtained by Eqs. (19,20,22) using the scalar and vector part of the potential from [35] and using the imaginary part of the potential $U(\mathbf{p}')$ given in [34]

$$W = \frac{\hbar c}{2} \rho_{\text{nucl}} \sigma_{NN} \frac{|\mathbf{p}'|}{E_{\mathbf{p}'}}, \tag{23}$$

where the values of ρ_{nucl} and σ_{NN} for ^{16}O are taken to be: $\rho_{\text{nucl}} = 0.16$ fm^{-3} and $\sigma_{NN} = 40$ mb.

As can be seen from Figures 7 and 8 the effects of accounting FSI are: the maximum of the scaling function decreases, while the tails of the scaling function for negative and positive values of ψ' increase. Also from Figure 8 can be seen the important role of the type of the time-independent optical potential used.
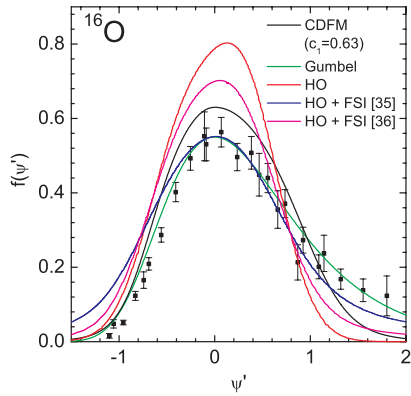
Figure 8. (Color online) The results for the scaling function $f(\psi')$ with and without accounting for the FSI using the spectral function in the Hartree-Fock method Eq. (15) with HO single-particle wave functions (for a given momentum transfer $q = 1$ GeV/c and energy of the initial electron $\epsilon = 1$ GeV) are compared with the experimental data, Gumbel distribution and CDFM result using $c_1 = 0.63$ [22].
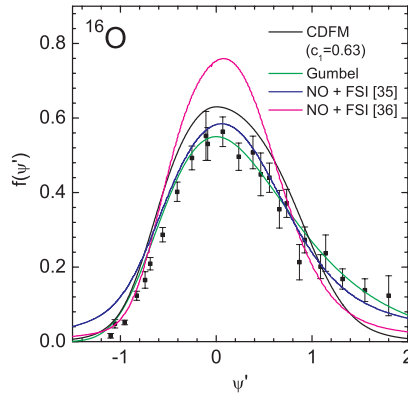
Figure 9. (Color online) The results for the scaling function $f(\psi')$ with accounting for the FSI using NO's from the Jastrow correlation method (for a given momentum transfer $q = 1$ GeV/c, energy of the initial electron $\epsilon = 1$ GeV, and parameters $\sigma_{1s} = 8.7$ MeV, $\sigma_{1p} = \sigma_{1d} = \sigma_{1f} = 0.5$ MeV) are compared with the experimental data, Gumbel distribution and CDFM result using $c_1 = 0.63$ [22].

The results in the case (ii) are presented in Figure 9 for a given momentum transfer $q = 1$ GeV/c and energy of the initial electron $\epsilon = 1$ GeV with accounting for the FSI (we consider two different types of the time-independent optical potential for ^{16}O the same as in the Figure 8). The results depend very weakly on the choice of parameters σ_i. There the value of the parameter σ_{1s} is fixed to be 8.7 MeV (that corresponds to the experimental width of the $1s -$ state in ^{16}O [36]) and the values of $\sigma_{1p} = \sigma_{1d} = \sigma_{1f} = 0.5$ MeV are fixed.

3 Conclusions

The results obtained show that:

1. The total momentum distribution (Figure 5) has a more realistic high-momentum tail when NO's obtained from the Jastrow correlation method.

2. In the case of using NO's, the behavior of $f(\psi')$ (Figure 4) is quite similar to that from our calculations using HO single-particle wave functions. A weak asymmetry of $f(\psi')$ exists but the results do not reproduce the experimental scaling function.

3. The effects of accounting FSI are: the maximum of the scaling function decreases, while the tails of the scaling function for negative and positive values of ψ' increase.

4. The results for the scaling function reproduce better experimental data when we take into account the effects of FSI using the imaginary part of the potential $U(\mathbf{p}')$ given in [34].

References

[1] D.B. Day, J.S. McCarthy, T.W. Donnelly and I. Sick *Ann. Rev. Nucl. Part. Sci.* **40** (1990) 357.

[2] C. Ciofi degli Atti, E. Pace, and G. Salmè, *Phys. Rev. C* **36** (1987) 1208; *Phys. Rev. C* **39** (1989) 259; *Phys. Rev. C* **43** (1991) 1155.

[3] C. Ciofi degli Atti, D.B. Day, S. Liuti, *Phys. Rev. C* **46** (1992) 1045; C. Ciofi degli Atti and S. Simula, *Phys. Rev. C* **53** (1996) 1689; C. Ciofi degli Atti and G. B. West, *Phys. Lett. B* **458** (1999) 447.

[4] A.N. Antonov, P.E. Hodgson, and I.Zh. Petkov, *Nucleon Correlations in Nuclei*, Springer-Verlag, Berlin-Heidelberg-New York (1993).

[5] X. Ji, J. Engel, *Phys. Rev.* **C40** (1989) R497.

[6] Ciofi degli Atti, C.B. Mezzetti, *Phys. Rev. C* **79** (2009) 051302.

[7] A.N. Antonov, P.E. Hodgson, and I.Zh. Petkov, Nucleon Momentum and Density Distributions in Nuclei (Clarendon Press, Oxford, 1988).

[8] O. Bohigas and S. Stringari, *Phys.Lett. B* **95** (1980) 9.

[9] M. Jaminon, C. Mahaux and H. Ngo, *Phys. Lett. B* **158** (1985) 103.

[10] E. Moya de Guerra, P. Sarriguren, J.A. Caballero, M. Casas, and D.W.L. Sprung, *Nucl. Phys.* **A529** (1991) 68.

[11] A.N. Antonov, V.A. Nikolaev, and I.Zh. Petkov, *Bulg. J. Phys.* **6** (1979) 151; *Z. Phys. A* **297** (1980) 257; *ibid.* **304** (1982) 239; *Nuovo Cimento A* **86** (1985) 23; *Nuovo Cimento A* **102** (1989) 1701; A.N. Antonov, D.N. Kadrev, and P.E. Hodgson, *Phys. Rev. C* **50** (1994) 164.

[12] G.B. West, *Phys. Rep.* **18** (1991) 263.

[13] I. Sick, D.B. Day, and J.S. McCarthy, *Phys. Rev. Lett.* **45** (1980) 871.

[14] W.M. Alberico, A. Molinari, T.W. Donnelly, E.L. Kronenberg and J.W. Van Orden, *Phys. Rev. C* **38** (1988) 1801.

[15] M.B. Barbaro, R. Cenni, A. De Pace, T.W. Donnelly, and A. Molinari, *Nucl. Phys.* **A643** (1998) 137.

[16] T.W. Donnelly and I. Sick, *Phys. Rev. Lett.* **82** (1999) 3212.

[17] T.W. Donnelly and I. Sick, *Phys. Rev. C* **60** (1999) 065502.

[18] C. Maieron, T.W. Donnelly and I. Sick, *Phys. Rev. C* **65** (2002) 025502.

[19] A.N. Antonov, M.K. Gaidarov, D.N. Kadrev, M.V. Ivanov, E. Moya de Guerra, and J.M. Udias, *Phys. Rev. C* **69** (2004) 044321.

[20] A.N. Antonov, M.K. Gaidarov, M.V. Ivanov, D. N. Kadrev, E. Moya de Guerra, P. Sarriguren, and J. M. Udias, *Phys. Rev. C* **71** (2005) 014317.

[21] A.N. Antonov, M.V. Ivanov, M.K. Gaidarov, E. Moya de Guerra, P. Sarriguren, and J.M. Udias, *Phys. Rev. C* **73** (2006) 047302.

[22] A.N. Antonov, M.V. Ivanov, M.K. Gaidarov, E. Moya de Guerra, J.A. Caballero, M.B. Barbaro, J.M. Udias, and P. Sarriguren, *Phys. Rev. C* **74** (2006) 054603.

[23] J.A. Caballero, M.B. Barbaro, A. N. Antonov, M. V. Ivanov, T.W. Donnelly, *Phys. Rev. C* **81** (2010) 055502.

[24] S. Frullani and J. Mougey, *Adv. Nucl. Phys*. **14** (1984) 1.

[25] S. Boffi, C. Giusti, F.D. Pacati, M. Radici, *Phys. Rep.* **226** (1993) 1; *Electromagnetic Response of Atomic Nuclei* (Oxford University Press, Oxford, 1996).

[26] J.J. Kelly, *Adv. Nucl. Phys.* **23** (1996) 75.

[27] A.S. Raskin, T.W. Donnelly, *Ann. of Phys.* **191** (1989) 78.

[28] M.V. Stoitsov, A.N. Antonov and S.S. Dimitrova, *Phys. Rev. C* **48** (1993) 74.

[29] P.-O. Löwdin, *Phys. Rev.* **97** (1955) 1474.

[30] A.N. Antonov, M.K. Gaidarov, M.V. Ivanov, D.N. Kadrev, G.Z. Krumova, P.E. Hodgson, H.V. von Geramb, *Phys. Rev. C* **65** (2002) 024306.

[31] J. Carbonell and V.A. Karmanov, *Nucl. Phys.* **A581**, 625 (1995); J. Carbonell, B. Desplanques, V.A. Karmanov, and J.-F. Mathiot, *Phys. Rep.* **300** (1998) 215.

[32] Arthur M. Ankowski and J.T. Sobczyk, *Phys. Rev. C* **77** (2008) 044311.

[33] H. Horikawa, F. Lenz, and N.C. Mukhopadhyay, *Phys.Rev. C* **22** (1980) 1680.

[34] H. Nakamura, R. Seki,and M. Sakuda, *Nucl.Phys. B, Proc. Suppl.* **139** (2005) 201 (and references therein).

[35] E.D. Cooper, S. Hama, B.C. Clark, and R.L. Mercer, *Phys. Rev. C* **47** (1993) 297.

[36] G. Jacob and Th.A. Maris, *Rev. Mod. Phys.* **45** (1973) 6.